

**Scientific and Technological Alliance for Guaranteeing
the European Excellence in Concentrating Solar
Thermal Energy**



FP7 Grant Agreement number:

609837

Start date of project:

01/02/2014

Duration of project:

48 months

Project Deliverable 7.9:

Technical assessment on the TES systems based on thermocline storage integrating filler materials and industrial-scale design of a packed-bed thermal storage for CSP

WP7 – Task 7.3.4	Deliverable 7.9
Due date:	January/2017
Submitted	January/2017
Partner responsible	CRS4
Person responsible	Lorenzo Pisani
Contributing Partners:	CNRS, DLR, CRS4, CyI, ETHZ, SENER
Document version:	1
Reviewed/supervised by:	
Dissemination Level	PU

Table of Contents

Table of Contents	2
List of Figures	3
1. INTRODUCTION	4
2 EXPERIMENTAL CHARACTERIZATION	5
2.1 CNRS contribution: Wettability Effect on Heat Transfer between Filler Materials and HTFs in a Single Storage Tank.....	6
WETTABILITY	7
WETTABILITY TESTS	7
CONCLUSION.....	14
2.2 DLR contribution: Thermal Properties of Natural Fillers.....	15
3. MODELING	19
3.1 CRS4 contribution: Effects of Filler Particles Geometry on Transport parameters	20
3.2 CYI contribution : Algebraic Model and Sensitivity Analysis	22
The algebraic model.....	22
Sensitivity analysis.....	23
4. PILOT-SCALE DEMONSTRATION AND IMPACT ASSESSMENT	27
4.1 ETHZ contribution: Pilot Scale Demonstration and Industrial Scale Design of a Packed-Bed Thermal Storage for CSP	28
4.2 SENER contribution: Impact Assessment of using Thermoclines with Filler in Plant Operation ...	29

List of Figures

Figure 1. Representation of the sessile drop method and contact angle	7
Figure 2. Graph representing the change in the contact angle of Cofalit with temperature	8
Figure 3. Graph representing the change in contact angle of Blast Furnace Slag with temperature	9
Figure 4. Evolution of the contact angle between Coal Fly Ash and Salt drop	9
Figure 5. Evolution of the contact angle between Polished Cofalit and Salt drop	10
Figure 6. Comparison of the behavior of contact angles in function of the temperature for the different substrates	11
Figure 7 "Mean values (symbols) and ranges of variation (vertical bars) of thermal conductivity λ with temperature for (a) magmatic and metamorphic and (b) sedimentary rocks as well as mean values and ranges of variation of (c) specific heat capacity C_p at constant pressure and (d) thermal capacity ($\rho \times C_p$) as a function of temperature [...] for magmatic, metamorphic and sedimentary rocks. [...] – figure and caption cited from ref. [1].	15
Figure 8 Average heat capacity of two different basalt types and quartzite over temperature. Values were averaged from individual Cp measurement of eight basalt (H), eight quartzite and five basalt (R) samples. The Cp value of quartz at 560°C indicated with (*) has to be taken with care since it is close to the quartz inversion temperature (573°C).	16
Figure 9 Solid materials with different shapes: a) pebbles, b) wood chips, c) slate chips. From [Pugliese et al. 2012]	21
Figure 10 Different packing orientations of wood chips and slate chips. From [Pugliese et al. 2012]	21
Figure 11 Comparison of the model tortuosity values with the experimental ones form [Pugliese et al. 2012]	21
Figure 12 Validation of algebraic model by comparison with results from literature.	22
Figure 13 (left) Standard deviation vs. mean of the elementary effects, as evaluated using Morris' screening method. (right) First order and total sensitivity indexes from the Variance Based Sensitivity Analysis.....	25

1. INTRODUCTION

The fast development of renewable energy production, driven by photovoltaic and eolic, requires a parallel development of energy storage systems capable of filling the time gap between production and consumption. Such distance is progressively increasing with the percentage of renewable energy and, therefore, the storage costs are becoming a fundamental component of the energy economy.

At the today state of technology development, thermal energy storage (TES) is convenient with respect to the electrochemical one. Since thermal energy is an intermediate energy form of solar thermodynamic energy conversion and can be stored without additional transformation steps, solar thermodynamics with TES is a natural choice for energy production in the near future.

In view of the expansion of TES technology, is important to study further possible cost reductions of TES systems by reducing both the amount and the cost of heat storage materials (HSM). While heat transfer fluid (HTF) must have specific transport characteristics, HSM can be generic, very low cost, condensed phase materials.

The single storage tank with thermocline and low cost fillers requires a relatively low amount of HTF in the storage system, as most of the heat capacity is provided by the fillers and, therefore, is a promising TES technology.

Use of natural rocks or industrial wastes as filler material, can bring a further important cost reduction with respect to ad-hoc made materials as spherical pebbles.

The main goal of the present deliverable is to investigate the possible use of such low cost materials in thermal storage. In particular, since the chemical, physical and geometrical characteristics of the fillers can be extremely various, a special focus has been put on the definition of a general procedure to predict the possible use and the performances of candidate filler.

A general procedure has been identified and each of the partners has contributed to the development of one or more steps. In synthesis, the procedure is the following with, in parenthesis, the contributing partners:

1. Experimental check of chemical and physical compatibility between filler materials and HTF (CNRS,DLR)
2. Thermo-physical (heat capacity, heat conductivity and solid particle density as a function of temperature) and geometrical (average particle volume, surface per unit volume and elongation) characterization of the eligible fillers found in step (1) (DLR)
3. Calculation of macro-homogeneous transport parameters (heat exchange, permeability, thermal conductivity) by using the geometrical and thermo-physical characterization performed in step (2) (CRS4)
4. Thermocline simulations and system optimization by using the macro-homogeneous parameter evaluated in step (3) (CyI)
5. Laboratory scale experiments on the system optimized in step (4) (ETHZ)
6. Impact assessment (SENER)

In the next sections, such steps are shortly described, making, in particular, reference to the DOW, which is reported in italic.

2 EXPERIMENTAL CHARACTERIZATION

The compatibility between filler materials and HTF must be tested to assess the eligibility of fillers. A first compatibility requirement is the wettability of the fillers by HTF. CNRS has conducted tests of vitrified wastes wettability by oil and molten salts, which are reported in section 2.1.

The eligibility of fillers requires as well chemical and thermo-physical compatibility between HTF and filler materials. DLR has performed lab-scale material tests for the one tank thermocline-filler concept with the following materials: natural stone (Quartzite, Basalt) as filler and solar salt as HTF. The stability of these filler materials, as potential candidates to be used in thermocline storage concepts, was investigated in long term experiments up to 5.000h. Additional anionic traces in the melt as corrosion products from the filler due to the reaction of instable mineral species with nitrates/nitrites were identified. However, no impact on the thermal properties of the salt could be determined. These properties remain to be unchanged over a time frame up to 5.000h which is confirmed by relatively stable nitrate/nitrite ratios.

Further technical details of this study are described in the conference papers “Martin, C., et al. (2014) ASME 2014 8th Int. Conf. on Energy Sustainability, June 30-July 2, 2014, Boston, USA “ and “Bonk, A. et al. (2016) SolarPaces, Okt., Abu Dhabi.”

DLR has contributed also by measuring the thermo-physical properties of heterogeneous natural stones as reported in Section 2.2.

2.1 CNRS contribution: Wettability Effect on Heat Transfer between Filler Materials and HTFs in a Single Storage Tank

One of the key parameter controlling the storage performance during discharge is the heat transfer between the solid and the liquid phase. This task aims at studying the possible heat transfer limitation at the interface of storage materials wall and HTF by conducting high temperature wettability test. Various vitrified wastes (previously identified as interesting candidates for filler materials) with both oil and molten salts as HTF will be tested at high temperature. The knowledge of the wettability characteristics between HTF and filler materials will permit to specify the list of vitrified waste candidate for TES.

The purpose of this study is to determine the effect of the wettability of the materials by the heat transfer fluids on the entire heat transfer system. This will lead to a better understanding of the materials and a better rounded choice on which material is best suited for this application. The process that was followed was to first define wettability and see how and by what it can be affected. Then the wettability has been measured for all of the system combinations. For these tests, salt beads have been prepared in the solar furnace at Procédés Matériaux et Energies Solaires (PROMES) at Odeillo, France and the Industrial wastes were shaped. After completing the wettability tests, the contact angles were measured on a program called ImageJ. This program helps to enhance the quality of the pictures in order to be able to take the angle measurements in the most reliable way. After completing the tests, Blast Furnace Slag showed the highest wettability in all kinds of tests.

Energy storage is one of the biggest costs for the thermal power plants as it is mostly based on the solar salt that is imported from Chile. The cost of solar salt is relatively high at 630\$-945\$/ton. This solar salt has also other uses especially in agriculture and it is not a widely available resource. So the smaller the amount used in power plants, the better the situation gets, economically and ecologically. There are also researches that are being conducted in order to completely replace the solar salt with generally available materials like air, or some synthetic material that is cheap enough, with good thermal properties like the synthetic oil Jarytherm® DBT. Jarytherm DBT Oil will be used in the pilot-scale parabolic trough that is being built in PROMES laboratory in Odeillo, France.

In this pilot-scale parabolic trough, the thermal-energy storage system will consist of a one tank storage system (thermocline tank) that contains the heat transfer fluid in direct contact with the heat storage material.

The materials include vitrified wastes like Cofalit, Coal Fly Ash or Blast Furnace Slag. These materials are based on industrial wastes such as asbestos containing waste, coal ash from thermal power plants, slag from the metallurgical industry and other sources. These are highly available materials that can be purchased at a low cost (10\$/ton). About 80% ^[1] of the heat transfer fluid will be replaced with low-cost filler materials. This will also reduce the maintenance costs as the maintenance will be limited to a one tank system without all the connections between the 2 tank system that collects the hot fluid in one tank and the cold fluid in another. In our work, the studied heat transfer fluids will be solar salts and Jarytherm DBT oil. These heat transfer fluids will be tested to study their wettability with different materials such as Cofalit, Coal Fly Ash and Blast Furnace Slag.

Wettability tests will be performed on the different combinations of substrate/Heat Transfer Fluid (HTF) in order to extract the contact angle to help assess the effect of wettability on the heat transfer process between the HTFs and the different substrates.

WETTABILITY

Wettability is the ability of a certain liquid to propagate along the surface of a solid. It is affected by the surface free energy of the solid, the interfacial tension between the liquid and the solid, and the surface tension between the liquid and the gas. The interfacial tension is the tension needed to expand the contact surface between the liquid and the solid. This interfacial tension represents the bonds between the molecules of the liquid. If the interaction between the solid and the liquid was higher than the forces between the molecules the system will be wettable. If the forces between the liquid's molecules are higher than the interaction between the liquid molecules and the surface's molecules, the liquid would shrink up itself and form a high contact angle between the liquid and the surface giving thus a system that is not wetting or better known as hydrophilic. The contact angle is measured between the intersection line of the liquid drop and solid, and the tangent to the outer surface of the drop. If this angle is higher than 90° the system is not wettable, if the angle is lower than 90° the system is considered wettable and if the angle is lower than 10° the system is considered extremely wettable.

In the related experiments, the same method as the one represented in Figure 1 was used. It is called the sessile drop method, which consists on resting a drop of the fluid on the solid substrate and wait until it reaches equilibrium in order to measure the contact angle.

The contact angle is affected by several elements like the roughness of the surface, the reactivity between the substrate and the liquid, the size of the drop, the surrounding atmosphere and the temperature at which the experiments will be conducted.

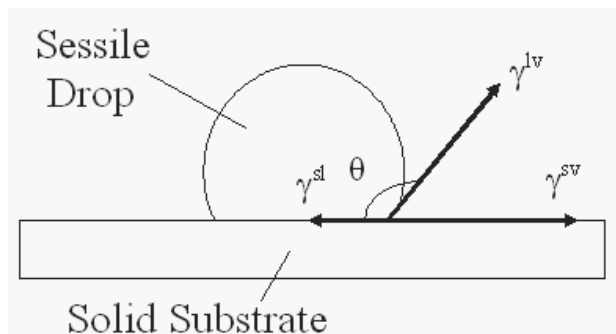


Figure 1. Representation of the sessile drop method and contact angle

WETTABILITY TESTS

The test bench consists of a tubular furnace that goes up in temperature with a predetermined step ($^{\circ}\text{C}/\text{min}$) as directed by the temperature regulator that regulates the increase in temperature. To start the experiments, for each system, salt was chosen to begin with. The heat transfer fluid was placed on the surface as close as possible to the center of the substrate, both of them were introduced in the tubular furnace and pushed to reach the center of the furnace where we will have the biggest temperature concentration with a minimal loss.

A camera was focused using the multifocal lens to get the best possible quality of image in order to study the evolution of the contact angle. After the end of all of the experiments, image analysis was done back at PROMES laboratory at Odeillo using image analysis program "ImageJ" that permits the user to change image properties like contrast and lighting effect and can also find the edges in the photos which makes the work easier. At the end of image enhancement and still in the ImageJ

program, lines are drawn to precise the limit between the substrate and the drop in order to measure the contact angle.

In the following parts, the different systems will be presented for the combination of different industrial wastes with solar salt at 500°C and 350°C and one case of Polished Cofalit with the Jarytherm DBT oil at 300°C. The tests for solar salt and oil were conducted at 500°C and 300°C respectively to mimic the case of normal use. The experiments with the solar beads at 350°C were accomplished to see if the contact angle of the system will be constant if left at a temperature between the melting and operating temperature, or it will wet the surface at the end of the experiment.

Results of the experiments with solar salt at 500°C

Cofalit + Solar Salt at 500°C

After insertion of the Cofalit/Salt sample and while heating the system up to 500°C, the salt begins to melt and form an elliptical shape with an evident contact angle. This contact angle decreases when the temperature increases until it reaches a value that cannot be measured by the program because of the high uncertainty, but it is a value that is lower than 5° which is already considered as extreme wettability. For the case of Cofalit it seems that it is extremely wettable with solar salt at 500°C.

Studying the graph in figure 2 we can see that the contact angle is slowly but steadily going towards the value of zero. The Cofalit/salt combination has the tendency to decrease the value of the contact angle linearly with the increase of temperature.

The curve at the end shows a clear tendency to continue decreasing even if it was at a slower rate than before.

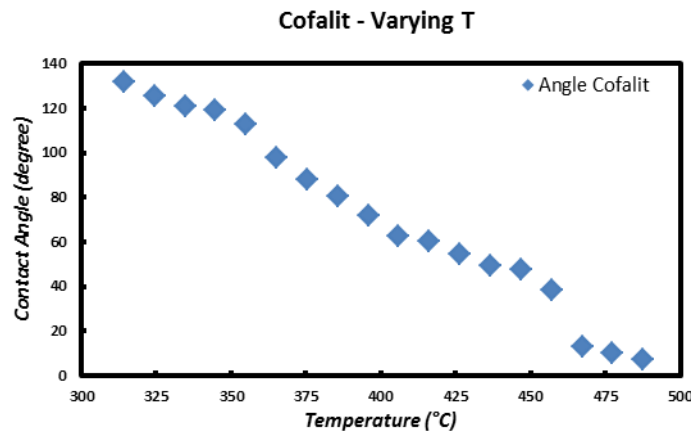


Figure 2. Graph representing the change in the contact angle of Cofalit with temperature

Blast Furnace Slag + Solar Salt at 500°C

The same procedure is followed for this experiment, and the contact angle also has the same tendency to decrease with the temperature. While it begins at 105° when it starts melting, the salt continues to expand the contact surface with the Blast Furnace Slag until the contact angle becomes 8° at the last measurement. The angle of 8° corresponds to a temperature of 471°C.

The curve shown in figure 3 gives a tendency to continue decreasing with temperature to achieve complete wettability at 500°C.

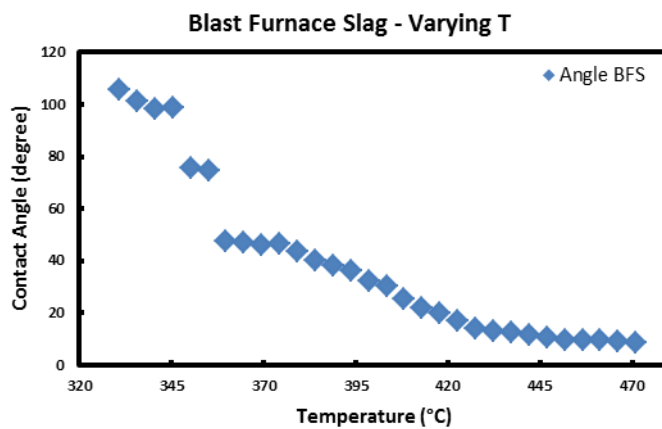


Figure 3. Graph representing the change in contact angle of Blast Furnace Slag with temperature

Coal Fly Ash + Solar Salt at 500°C

After insertion of the Coal Fly Ash/Salt sample the same process starts to take place and the salt bead starts to melt forming a contact angle of 131° after homogenization and begins to get smaller and smaller with time. But for the Coal Fly Ash a different process was seen as the salt bead starts to disappear in a fast manner.

On the camera feed a slight motion was detected as the salt drop migrated towards one of the sample's edges. After recovery of the sample a wet spot was detected at its edge.

The experiment was repeated after taking good measures to ensure the well centering of the salt bead and secure the horizontality of the whole system. The same behavior of the drop was observed and it disappeared in a fast manner once it started melting, which led to the conclusion that the salt drop is being absorbed by the Coal Fly Ash.

Studying the graph shown in figure 4, which was performed for the second trial, we can see that at the homogenization point of the drop at almost 300°C, the contact angle is 131°. It starts to decrease normally until a temperature of about 360°C, where it plummets to the value of zero in an interval of temperature of 20°C. The drop completely disappears at the temperature of 380°C.

The roughness of Coal Fly Ash is almost double the values of the other materials. We can deduce that this high value of roughness might be caused by the high porosity of the material which will affect both the roughness, and the ability of the material to absorb the liquid drop.

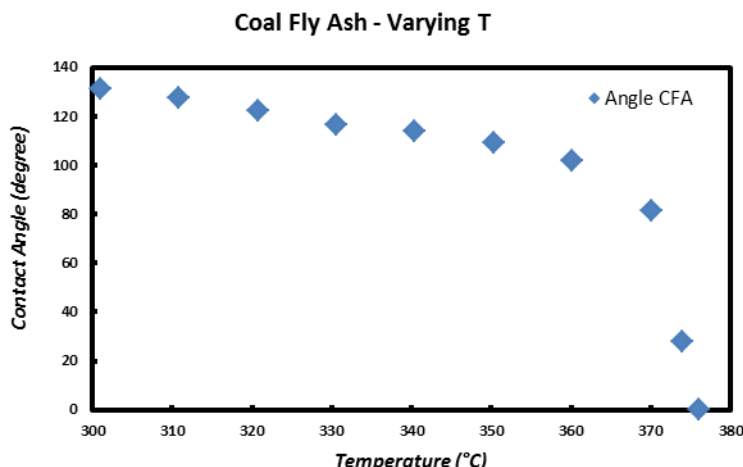


Figure 4. Evolution of the contact angle between Coal Fly Ash and Salt drop

Polished Cofalit + Solar Salt at 500°C

After insertion of the Polished Cofalit/Salt sample the same heating process takes place and the salt bead starts to melt forming a contact angle of 103° after homogenization and begins to get smaller and smaller with time.

This contact angle decreases when the temperature increases until it reaches a value that cannot be measured by the program because of the high uncertainty, but as for the normal Cofalit sample it has a value that is lower than 5° which is already considered as extreme wettability. For the case of Polished Cofalit it seems that it will eventually reach extreme wettability with solar salt at 500°C. Salt residues appear on most of the sample's surface after cooling which means that it has propagated along the whole surface, reaching a contact angle of zero.

Studying the graph in figure 5 we can see that the contact angle is slowly going towards the value of zero until reaching it after a small amount of time (couple of minutes) at a temperature of 500°C.

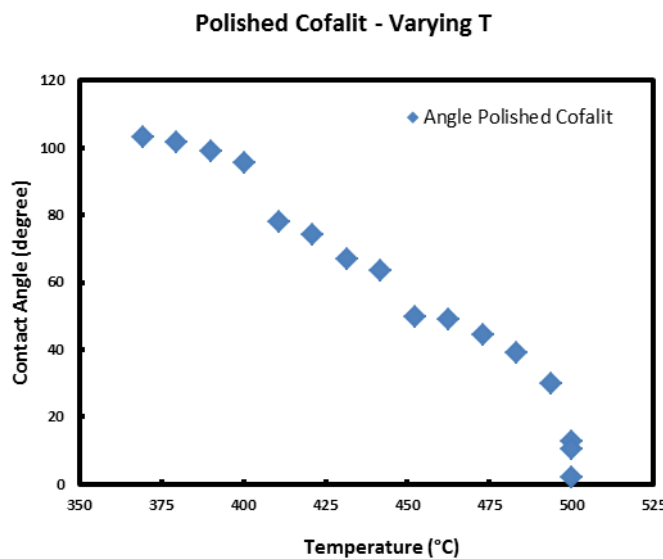


Figure 5. Evolution of the contact angle between Polished Cofalit and Salt drop

Comparison Between Different Industrial Wastes at 500°C

Comparing the different curves on figure 6, it is clear that all of the industrial wastes show great wettability properties at 500°C. The Blast Furnace Slag tends to extreme wettability in an exponential manner after it starts to melt and homogenize. Cofalit tends linearly to its extreme wettability condition like the Polished Cofalit that tends linearly towards extreme wettability at 500°C. For the Coal Fly Ash we cannot see a tendency profile as the drop is absorbed after a small interval of increment in temperature.

Blast Furnace Slag shows the fastest way to reach extreme wettability with a difference of almost 30° most of the time with the contact angle of the Cofalit and more than 45° with the contact angle of Polished Cofalit. Hence we can conclude that the Blast Furnace Slag is the most convenient for this application, wettability-wise.

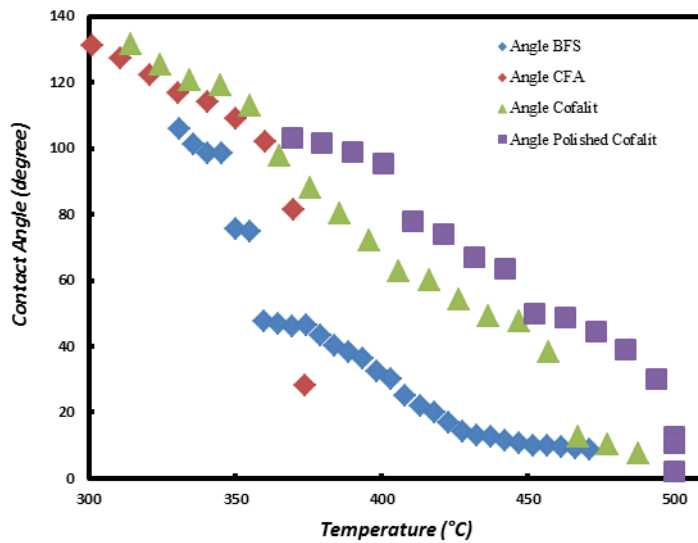


Figure 6. Comparison of the behavior of contact angles in function of the temperature for the different substrates

Results of the experiments with solar salt at 350°C

The main purpose of these experiments was to study the ability of the salt drop to completely wet the surface at a relatively low temperature or if it would keep a constant value of the contact angle after being left at the temperature of 350°C for 30 minutes.

After completing the experiments, all of the samples showed consistency when it came to the result, that the contact angle would decrease until a certain limit where it becomes stable. This meant that there will be a difference in the contact angle at temperatures lower than 500°C. The results will be shown in the upcoming sections.

Cofalit + Solar Salt at 350°C

When the salt begins to melt the contact angle starts at 134° and keeps decreasing with the temperature increment until it reaches its lower limit of 83.86° after 30 minutes at 350°C.

After extraction of the Cofalit/Salt bead combination, the salt bead forms an elliptical shape on the surface of the Cofalit sample as the shape that was seen during the melting process, with an angle that can be distinguished just by looking at the system.

Figure 7 shows the tendency of the system to reach a constant contact angle at 350°C after a certain amount of time. After homogenization of the salt drop at 1763 seconds, the initial contact angle is 134°. This angle keeps decreasing with time and temperature until it reaches its lower limit.

The variation of the contact angle at 350°C begins fast but once it starts to lean towards the limits, it stabilizes around the value of 83°. Although the curve shows a tendency to continue decreasing, this tendency is very slow and most probably will reach a limit that is very close to 83° as the decrease in contact angle becomes almost insignificant after about 10 minute of the beginning of the temperature stabilization process.

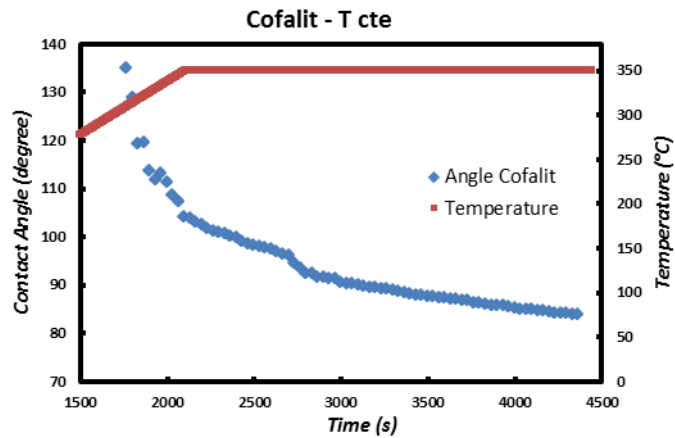


Figure 7. Evolution of the contact angle between Cofalit and Salt drop at a temperature of 350°C

Coal Fly Ash + Solar Salt at 350°C

When the salt begins to melt the contact angle starts at 143° and keeps decreasing with the temperature increment until it disappears completely after 16 minutes of its homogenization and after 9 minutes of temperature stabilization at 350°C.

The graph represented in figure 8 shows the variation of the contact angle before the disappearance of the salt drop. This angle starts decreasing with temperature and time until a certain point where it falls directly from a high value to disappearance. Although the contact angle decrease is not related with the time spent at the stable temperature of 350°C, it implicates that Coal Fly Ash will absorb the salt bead at any temperature and that it is not affected by the value of the temperature but with its own high porosity.

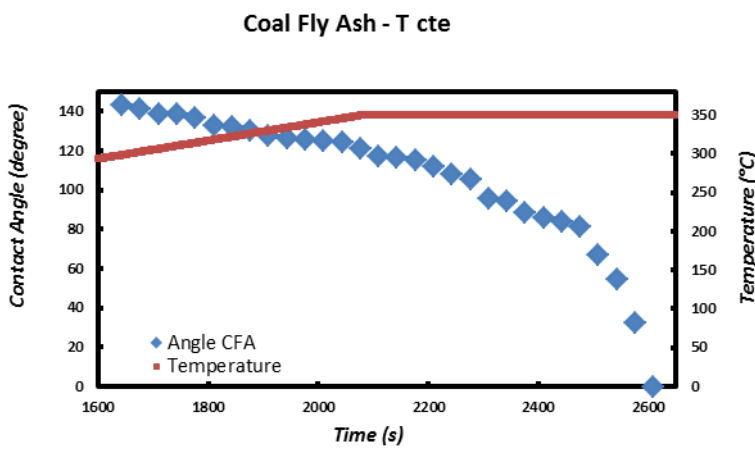


Figure 8. Evolution of the contact angle for Coal Fly Ash and Salt drop at a temperature of 350°C

Blast Furnace Slag + Solar Salt at 350°C

When the salt begins to melt the contact angle starts at 132° and keeps decreasing with the temperature increment until it reaches its lower limit of 40.5° after 30 minutes at 350°C. After extraction of the Blast Furnace Slag/Salt bead combination, the salt bead forms an elliptical shape on the surface of the Blast Furnace Slag sample as the shape that was seen during the melting

process. It can be clearly seen that it is lower than the contact angle between Cofalit and the salt drop.

Figure 9 shows the tendency of the system to reach a constant contact angle at 350°C after a certain amount of time. After homogenization of the salt drop at 1733 seconds, the initial contact angle is 132°. This angle keeps decreasing with time and temperature until it reaches its lower limit. The variation of the contact angle at 350°C begins fast but once it starts to lean towards the limits, it stabilizes around the value of 40°.

The slow transition in the contact angle's value at the end of the experiment indicates the tendency of the salt drop to reach a stable angle at the temperature of 350°C.

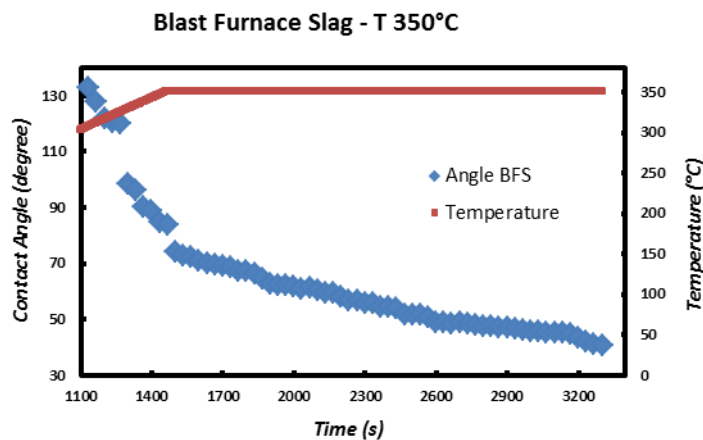


Figure 9 .Evolution of the contact angle for Blast Furnace Slag and Salt drop at 350°C

Comparison Between Different Industrial Wastes at 350°C

Comparing the different curves on figure 10, it is clear that all of the industrial wastes tend to have a constant contact angle with the heat transfer fluid at 350°C. Both of the Cofalit and Blast Furnace Slag tend to a constant angle in an exponential manner after they start to melt and homogenize. For the Coal Fly Ash we cannot see a tendency profile as the drop is absorbed after a small interval of temperature stabilization.

Blast Furnace Slag reaches the lowest contact angle compared to the Cofalit, almost half of the Cofalit's contact angle. This means that the Blast Furnace Slag will reach complete wettability before the Cofalit. Again the Blast Furnace Slag proves to be the best material wettability-wise.

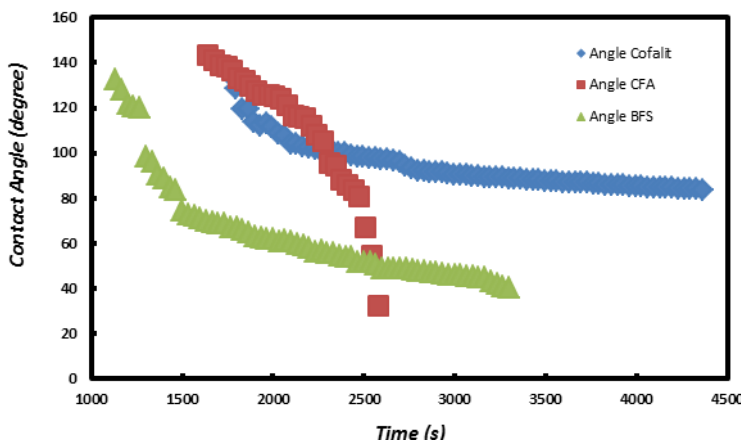


Figure 10.Comparison of the contact angle in function of time for different substrates at 350°C

Results of the experiments with Jarytherm DBT Oil

To begin with this experiment, it was needed to put the oil on the substrates before introducing them in the furnace. While completing this step it was obvious that the oil with all of the samples was highly wettable at ambient temperature. One exception was made for the Coal Fly Ash as it absorbed the oil instantly after putting it on the substrate. When this was observed it was decided to complete the experiment with only the polished Cofalit as it appeared to have the highest contact angle, and could thus be considered as representative to all of the systems if it reached complete wettability at 300°C. After extraction of the sample from the furnace, it is clear that the drop spread on a big surface of the polished Cofalit and there is no sign of the initial drop which signifies a very good wettability as we are still far from the evaporating temperature of the oil.

Studying the graph in figure 11 it is observed that the contact angle at ambient temperature is about 21°C.

The contact angle decreases in a slow manner at the beginning and then drops about the half of its value around 250°C. The measurements stop at 8° for 284° as the angles become harder to distinguish after this temperature

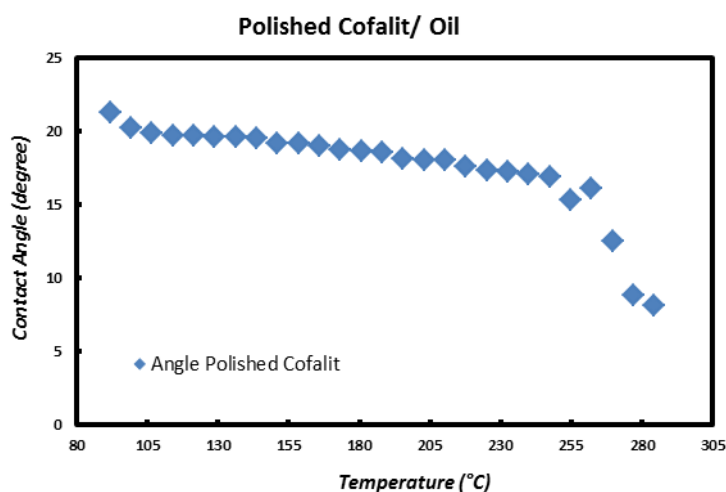


Figure 11. Evolution of the contact angle between polished Cofalit and Jarytherm DBT Oil

CONCLUSION

After all of these experiments, it is obvious that the Blast Furnace Slag is the most wettable between these elements and the most adaptable if only wettability is taken into account. These results are not the only criteria that should be considered for the choice of the final industrial waste to be used. A study of the complete heat transfer and energy storage capacity should be conducted as it would yield a better understanding of the heat storage system in order to store the highest possible amount of energy. Using this study we can infer compromises between different characteristics of the materials including the wettability.

Coal Fly Ash in its current form should not be considered for the energy storage application, as it showed an extremely high tendency to absorb the heat transfer fluid.

The ability of Coal Fly Ash to absorb the fluids indicates that a higher amount of fluids have to be used to fill the system.

The decision over which material to use may depend also on the size of the thermal energy storage tank and even the way of use.

2.2 DLR contribution: Thermal Properties of Natural Fillers

DLR will perform lab-scale material tests with low cost filler materials

The earth crust is made up by a large number of different rock types typically classified as sedimentary rocks, metamorphic rocks or igneous rocks depending on their formation history. Sedimentary rocks (e.g. sandstones and chalks) are formed by deposition and cementation of materials on the earth's surface or within bodies of water. They make up only 8% of the earth's crust and cover up metamorphic and igneous rocks. Metamorphic rocks are formed from sedimentary rocks by heat and pressure, typically $T > 150^\circ\text{C}$ and $P \sim 1500\text{bar}$, motivating thorough chemical and physical changes. However, not all constituents of metamorphic rocks have necessarily formed by the metamorphic process. Olivines, quartz and pyroxenes – all major components in basalt rocks – typically remain chemically unchanged during metamorphism. Igneous or magmatic rocks are formed by cooling and subsequent solidification of magma or lava. The melting of existing rocks in the first place is motivated by one or more changes of either temperature; pressure or compositional changes. The formed rocks can possess exceptional compressive strength (up to 400 MPa) which at the same time can vary significantly depending on the rocks composition. A selection of literature data on general thermo-physical properties is presented in Figure 7 comprising temperature dependent thermal conductivity, heat capacity and thermal capacity for sedimentary, magmatic and metamorphic rocks.

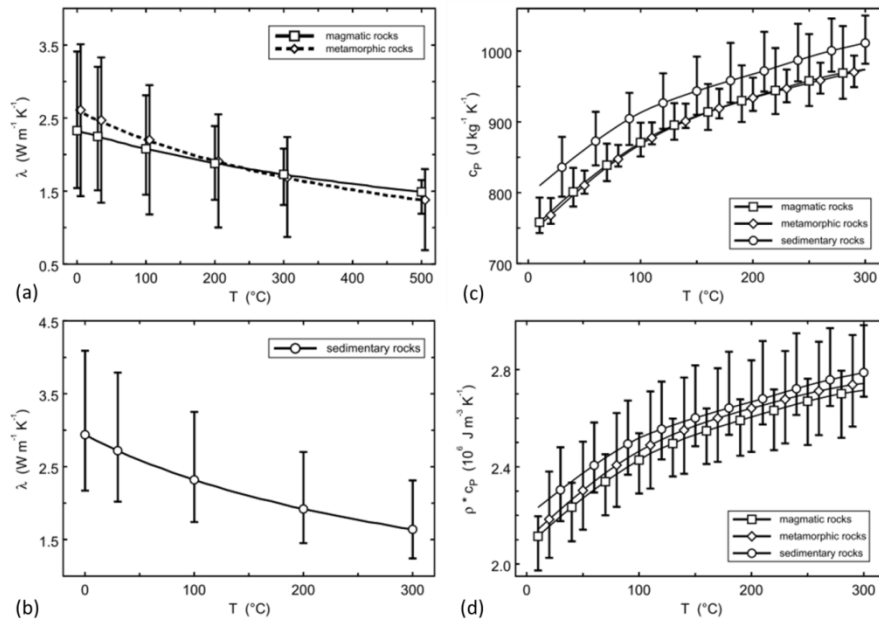


Figure 7 "Mean values (symbols) and ranges of variation (vertical bars) of thermal conductivity λ with temperature for (a) magmatic and metamorphic and (b) sedimentary rocks as well as mean values and ranges of variation of (c) specific heat capacity C_p at constant pressure and (d) thermal capacity ($\rho \times C_p$) as a function of temperature [...] for magmatic, metamorphic and sedimentary rocks. [...]" – figure and caption cited from ref. [1].

Thermal properties of natural stones can be found in different mineral databases although the majority is measured under non-ambient pressures. Data published in *Applied Geothermics* is based on unpressurised measurements and summarizes other literature data. Potential natural rock candidates for thermocline or sensible heat storage have been identified prior to this report and are presented in ref. [2] and are quartzite, basalt and diabas. Typical compositions of the rocks are presented in Table 1. Obviously, the exact composition depends on the mining area and has a direct impact on the thermo-mechanical properties. Therefore, some properties cannot be generalized, such as temperature specific weight loss (indicating thermal stability) since they depend on the exact composition of the rock. Consequently, it is recommended to measure relevant properties

using natural rocks of a close-by mining area which, in case of DLR, are the strip mining area Hühnerberg and Rossdorf.

Table 1 Typical composition of three potential natural rocks to be used in sensible or thermocline storage concepts

	Basalt	Quartz	Diabas
Plagioclase feldspar	16-60%	-	25-47%
Alkali feldspar	0-12.5%	-	
Quartz	0-6%	> 98%	28-53%
Mafic minerals	40-70%	-	-
Glimmer	-	-	4-21%
Chlorite	-	-	4-25%
Carbonates	-	-	0-6%
Common accessory constituents	Hornblende, pyroxenes, biotite, olivine, magnetite, ilmenite, apatite	-	<i>same as basalt</i>

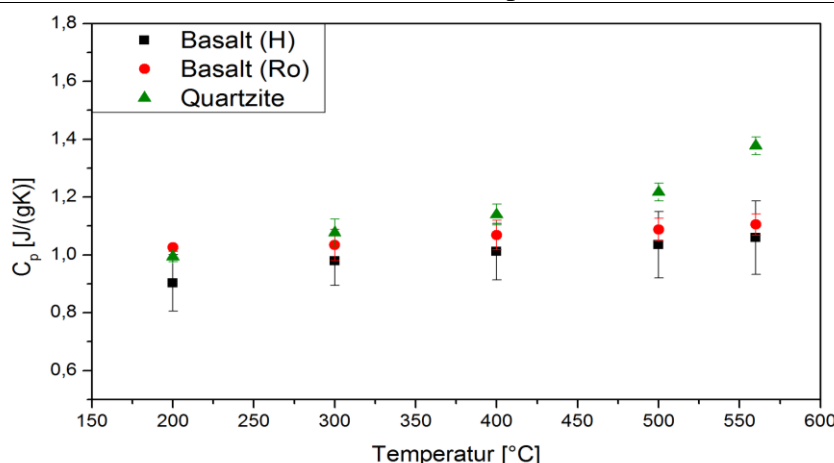


Figure 8 Average heat capacity of two different basalt types and quartzite over temperature. Values were averaged from individual Cp measurement of eight basalt (H), eight quartzite and five basalt (R) samples. The Cp value of quartz at 560°C indicated with (*) has to be taken with care since it is close to the quartz inversion temperature (573°C).

For sensible and thermocline concepts the heat capacity (C_p) is one of the most crucial properties since it directly affects the storage capacity of the system. The heat capacities of two basalt types and quartz rock have been analyzed using DSC analysis following ASTM 1269-11 and averaged data of a minimum of 5 measurements for each rock is presented in Figure 8. The C_p of both basalt types can be considered equal within the experimental error over a temperature range of 200°C to 560°C. In both cases it remains almost constant at temperatures higher than 400°C. Quartz samples have a steadily increasing C_p over temperature which is slightly higher than those of both basalt samples.

The heat conductivity of minerals is one of the major properties affecting the thermal dissipation of heat in thermocline or sensible heat storage systems. Differences in the local environment of the rock compartments can however dramatically affect thermal conductivity, e.g. a higher quantity of quartz (~7.69 W/(mK)) instead of albite (2.14 W/(mK)) increases the thermal conductivity of quartzite dramatically. In a similar fashion water content at lower temperature and porosity affect thermal conduction, which is however only relevant at temperatures below 300°C. Yet, *average* values of 2.11 W/(mK) for basalt, 5.00 W/(mK) for quartzite and 2.50 W/(mK) for diabase

(greywacke) are common at room temperature.[3] Kappelmeyer and Hänel describe that the thermal conductivity decreases with increasing temperature up to the melting point (Kappelmeyer and Hänel 1974). In quartzite for example, the thermal conductivity drops from more than 5 W/(mK) at R.T. to 3.6 W/(mK) at 200°C.

The thermal expansion (CTE) typically varies between 5.5 and 11.5E-6*K⁻¹ at 25°C for quartzite, basalt and other siliceous minerals. Values can undergo significant changes due to the heterogeneous nature of the minerals themselves being mainly orientation phenomena, inhomogeneities, compositional changes and other microscopic properties such as grain size and silica content.[4] At temperatures above 500°C not only the CTE can increase markedly but abrupt structural transitions can occur. One of the most extensively analyzed phenomena is quartz inversion, a structural transition from α- to β-SiO₂, occurring in quartz minerals at ~573°C resulting in (isotropic) expansion by 0.45%. [5] Consequently, minerals or rocks partially consisting of quartz typically exhibit a jump in the CTE at 573°C. Overall, the CTE of rocks is quite small making values such as the density almost independent of temperature. Vosteen and Schellschmidt therefore suggest accepting density values as constant over temperature ranges.[1]

Table 2 Part 1 of recommended thermo-physical properties of natural rocks measured in this report or from literature data. Values marked grey and black represent values for specific rock samples and general values for this rock type, respectively.

Mineral / Stone	Density at 25°C [kg/m ³]	Heat Capacity [J/(gK)]	Thermal conductivity [W/m°C]
Quartz (99%SiO ₂)	2630*	0.846+7.41E-4*T(°C) **	7.8-1.8E-2*T(°C)+1.8E-5[T(°C)] ² [6]*** (-50 < T < 900°C)
Basalt (R)	2900 [7]	0.87+3.89E-4*T(°C) **	7.8-1.8E-2*T(°C)+1.8E-5[T(°C)] ² [6]***
Basalt (H)	3031*	0.958+2.63E-4*T(°C) **	7.8-1.8E-2*T(°C)+1.8E-5[T(°C)] ² [6]***
Diabas	2750 [8,9]**	0.741+5.366E-4*T(°C) [9]	3.77*[T(°C) ^{^(-0.25)}] [3]***
Basalt (general)	2950 [8]**	0.956+2.011E-4*T(°C) [10] 0 < T < 900°C	1.35+7.5E-4*T(°C) [9]*** (0 < T < 1000°C)
100% SiO ₂	2650 [3]	0.815+8.27E-4*T(°C) (0-900°C) [11]	7.8-1.8E-2*T(°C)+1.8E-5[T(°C)] ² [6]***

*: from technical datasheet

**: interpolation from literature by DLR for this report

***: at 5 MPa

#: consider data of the general mineral

Table 3 Part 2 of other recommended thermal and mechanical properties of natural rocks measured in this report or from literature data. Values marked grey and black represent values for specific rock samples and general values for this rock type, respectively.

Füller	CTE [10-6K-1] from 20-1000°C	Compressive Strength at 25°C [N/mm ²]	Flexural strength at 25°C [N/mm ²]	Mass loss up to 900°C [wt%]
Quartz (99%SiO ₂)	49.8 [9]	150 – 250 [8] [†]	11 – 25 [8] [†]	< 0.1 [2]
Basalt (H)	5.4 [12]	150 – 300 [8] [†]	13 – 25 [8] [†]	1.97 [2]
Basalt (R)				
Diabas	~18 (25-200°C) [13]	150 – 250 [8] [†]	13 – 25 [8] [†]	9.01 [2]
Basalt (other)	~8 [10]	290 – 400 [8] [†]	-	-
100% SiO ₂	49.8 [9]	150 – 250 [8] [†]	11 – 25 [8] [†]	0 %

[†]: accurate values require measurements of rocks from the specific mining areas.

References

- [1] H.-D. Vosteen, R. Schellschmidt, Influence of temperature on thermal conductivity, thermal capacity and thermal diffusivity for different types of rock, *Phys. Chem. Earth, Parts A/B/C.* 28 (2003) 499–509. doi:10.1016/S1474-7065(03)00069-X.
- [2] C. Martin, N. Breidenbach, M. Eck, Screening and Analysis of Potential Filler Materials for Molten Salt Thermocline Storages, in: Vol. 1 Comb. Energy Cycles, CHP, CCHP, Smart Grids; Conc. Sol. Power, Sol. Thermochem. Therm. Energy Storage; Geothermal, Ocean. Emerg. Energy Technol. Hydrog. Energy Technol. Low/Zero Emiss. Power Plants an, ASME, 2014: p. V001T02A025. doi:10.1115/ES2014-6493.
- [3] L. Eppelbaum, I. Kutasov, A. Pilchin, Thermal properties of rocks and density of fluids, in: *Appl. Geotherm.*, Springer Berlin Heidelberg, Berlin, Heidelberg, 2014. doi:10.1007/978-3-642-34023-9.
- [4] Z.P. Bazant, M.F. Kaplan, *Concrete at High Temperatures: Material Properties and Mathematical Models*, Longman, 1996.
- [5] D.R. Lide, *CRC Handbook of Chemistry and Physics*, 76th edition, 2003.
<http://oem.bmjjournals.org/cgi/doi/10.1136/oem.53.7.504>.
- [6] H. Kanamori, N. Fujii, H. Mizutani, Thermal diffusivity measurement of rock-forming minerals from 300° to 1100°K, *J. Geophys. Res.* 73 (1968) 595–605. doi:10.1029/JB073i002p00595.
- [7] E. Stolper, D. Walker, Melt density and the average composition of basalt, *Contrib. to Mineral. Petrol.* 74 (1980) 7–12. doi:10.1007/BF00375484.
- [8] DIN 52100-2 - Naturstein - Gesteinskundliche Untersuchungen - Allgemeines und Übersicht, 2007.
- [9] E.C. Robertson, Thermal properties of rocks - Report 88-441, 1988.
- [10] P. Hartlieb, M. Toifl, F. Kuchar, R. Meisels, T. Antretter, Thermo-physical properties of selected hard rocks and their relation to microwave-assisted comminution, *Miner. Eng.* 91 (2016) 34–41. doi:10.1016/j.mineng.2015.11.008.
- [11] M.W. Chase Jr., NIST-JANAF Thermochemical Tables, *J. Phys. Chem. Ref. Data.* 9 (1998) 1–1951.
- [12] E.B. Dane Jr, Density at High Temperature; Thermal Expansion, in: F. Birch, J.F. Schairer, H.C. Spicer (Eds.), *Handb. Phys. Constants*, 36th ed., Geological Society of America Special Papers, 1942: pp. 27–37.
- [13] D. Richter, G. Simmons, Thermal expansion behavior of igneous rocks, *Int. J. Rock Mech. Min. Sci. Geomech. Abstr.* 11 (1974) 403–411. doi:10.1016/0148-9062(74)91111-5.

3. MODELING

Macro-homogeneous models, describe the porous media as continuum media with ad-hoc averaged parameters describing their complex multiphase structure. This approach has the advantage of describing the system geometry at the tank level, ignoring the details of the single filler particles. Within this approach, the evolution of solid and fluid phase's temperatures T , noted by subscripts s and f respectively, inside the tank, can be described by the following equations:

$$\begin{aligned} \varphi_f c_f \left(\frac{\partial T_f}{\partial t} + v \nabla T_f \right) &= k_f \nabla^2 T_f + h_{sf} a_{sf} (T_s - T_f) \\ (1 - \varepsilon) \rho_s c_s \frac{\partial T_s}{\partial t} &= k_s \nabla^2 T_f - h_{sf} a_{sf} (T_s - T_f) \end{aligned}$$

where: ε is the porosity, ρ the density, c the heat capacity, v the fluid velocity, k the thermal conductivity h the heat transfer coefficient and a the pore surface per unit volume.

In the equations above, all the complexity of the porous structure, including the geometry of the filler particles and their packing characteristics (density and orientation), is left to the evaluation of the averaged k and h parameters.

In the state of the art models, such dependence is well characterized for spherical particles only and is expressed in terms of their diameter and packing density. The effects of using non spherical particles fillers, as natural rocks or industrial wastes, on the thermocline characteristics, cannot be modeled without properly adjusting the transport parameters. This gap has been filled by a geometrical model developed at CRS4, which is described in section 3.1.

Numerical resolution of the macro-homogeneous equations above can be still computationally heavy because of the time scale differences between the physical processes of heat transfer and conduction and the system operation times which can run through hours or days. At CyI, a new algebraic approach to simplify the numerical resolution of such equations has been developed and applied to the sensitivity analysis of thermoclines. The model is described in section 3.2.

3.1 CRS4 contribution: Effects of Filler Particles Geometry on Transport parameters

CRS4 will extend its simulation tools originally developed to describe one-tank thermal storage with pebbles as storage materials and gas mixtures as HTF

State of the art models for the description of TES thermocline system with fillers consider spherical filler particles only. The effects of using filler particles of different shape on the transport parameters is unknown and the corresponding thermocline characteristics cannot be predicted properly.

In order to fill this gap, CRS4 researchers developed a model to evaluate the transport properties of a fluid through media formed by packing particles of general shape and orientation.

In general, the physical interactions of a solid medium with a fluid can be described through 3 main parameters: the porosity ε , which represents the space fraction available to the fluid flow, the pore surface per unit volume a , which gives a measure of the solid-fluid interactions and the tortuosity τ , which gives a measure of the length of the path that the fluid must run to cross the porous medium. Once these parameters are known, the transport parameters as the conductivity k , the permeability K and pore velocity v , can be rescaled according to:

$$k = \frac{\varepsilon}{\tau} k_{\text{void}}$$

$$K = \frac{\varepsilon^3}{c \tau^2 a^2}$$

$$v = \frac{\tau}{\varepsilon} v_{\text{void}}$$

While ε and a can be easily evaluated by measuring average surface, volume and packing density of the single fillers particles, evaluation of the tortuosity requires knowledge of filler shape and orientation.

The dependence of the tortuosity on the filler particles geometry is the subject of the study “A Geometrical Study of the Tortuosity of Anisotropic Porous Media” published in *Transport in Porous Media* [Pisani 2016]. In this work, the dependence of tortuosity on the geometrical structure of a porous medium is studied. In particular, the considered porous media have anisotropic structures, being composed by a collection of object of similar shape, with a well-defined orientation.

Geometrical expressions for the tortuosity as a function of the porosity, of shape factors characterizing the geometry of the solid objects and of the orientation of the flow with respect to the object axes are derived. The tortuosity expressions are validated through a series of numerical simulations of diffusion phenomena, finding a good agreement. The model is also compared with experimental data from literature, showing its possible use in the prediction of the transport properties of a porous medium made by assembling similar solid particles, by a simple geometrical characterization of its components.

In Fig. 1, examples of possible fillers of different shape are shown. The packing of these particles can be either isotropic or ordered along specific orientations, as exemplified in Fig. 2.

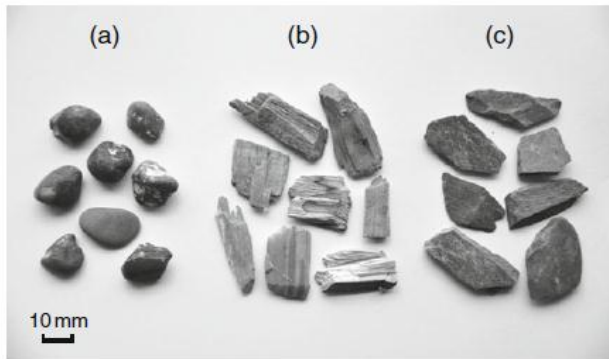


Figure 9 Solid materials with different shapes: a) pebbles, b) wood chips, c) slate chips. From [Pugliese et al. 2012]

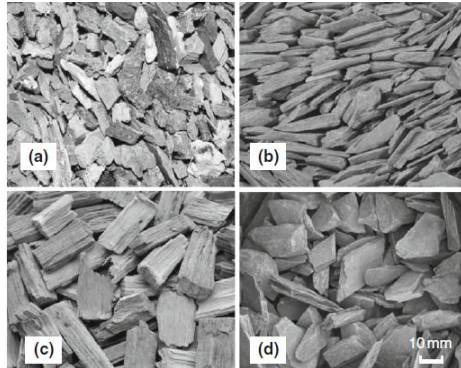


Figure 10 Different packing orientations of wood chips and slate chips. From [Pugliese et al. 2012]

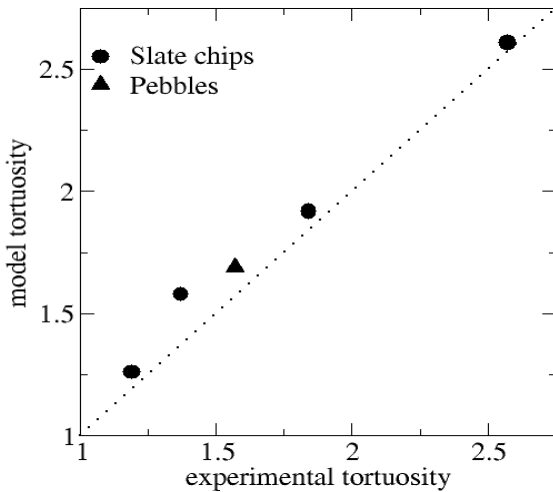


Figure 11 Comparison of the model tortuosity values with the experimental ones form [Pugliese et al. 2012]

In Fig. 3, the experimental tortuosity values of the media depicted in Fig. 2, are compared with the modeled ones. It is seen that the model provides an excellent estimate of the tortuosity at the price of a very simple characterization of the average particles geometry. Note that changes in the particles shape and orientations can change the tortuosity by a factor of two or more; the transport parameters change correspondingly. For example, within this set of particles, the permeability varies by a factor of four, with important consequences on the pumping energy.

All the details of the model are published in [Pisani 2016]

References

1. L. Pisani, "A Geometrical Study of the Tortuosity of Anisotropic Porous Media" *Transport in Porous Media*, 114 (1), 201-211 (2016)
2. L. Pugliese, T. G. Poulsen, R. R. Andreasen, *Water Air Solid Pollut.* 223, 4101 (2012)

3.2 CYI contribution : Algebraic Model and Sensitivity Analysis

CYI will use simulations, including CFD calculation to perform a sensitivity analysis on various influences on thermocline storage tanks, such as filler particle size, porosity, material properties and heat transfer characteristics.

The algebraic model

The one-dimensional two-phase energy equations for the solid and filler materials of the thermocline tank are simplified through the derivation of an algebraic model that captures the transient nature of the evolution of both solid and filler material temperatures, given by:

$$\theta_f = \frac{1 \pm \text{sign}(\zeta - \gamma_f \text{Pe})}{2} \sqrt{1 - \exp\left(\frac{-(\zeta - \gamma_f \text{Pe})^2}{(\pi D^\star \tau)}\right)},$$

$$\theta_s = \theta_f + \frac{\gamma_f \gamma_s \text{Pe}}{\text{Bi} \sqrt{4\pi D^\star \tau}} \exp\left(\frac{-(\zeta - \gamma_f \text{Pe})^2}{(\pi D^\star \tau)}\right).$$

where the following non-dimensional parameters have been introduced:

$$\theta = \frac{T - T_c}{T_h - T_c}, \quad \zeta = \frac{z}{L} \quad \text{and} \quad \tau = \frac{tk_{\text{eff}}}{L^2 (\rho C_p)_{\text{eff}}} \quad \gamma_f = \frac{\epsilon (\rho C_p)_f}{(\rho C_p)_{\text{eff}}}, \quad \gamma_s = \frac{(1 - \epsilon) (\rho C_p)_s}{(\rho C_p)_{\text{eff}}},$$

$$\beta_f = \frac{\epsilon k_f}{k_{\text{eff}}}, \quad \beta_s = \frac{(1 - \epsilon) k_s}{k_{\text{eff}}}, \quad \text{Pe} = \frac{uL (\rho C_p)_{\text{eff}}}{\epsilon k_{\text{eff}}}, \quad \text{Bi} = \frac{6(1 - \epsilon) k_f \text{Nu} L^2}{k_{\text{eff}} d_p^2},$$

The strength of this model over other one-dimensional models in the literature is that it accurately captures the importance of the diffusion term [Votyakov 2014] and is an algebraic model and hence much faster in its evaluation as compared to the original differential equation [Votyakov 2015]. Further, an excellent agreement between predictions of the algebraic model as compared to those of CFD simulations in the literature [Yang 2010, Hanchen, 2011] was found, as shown in Figure 12.

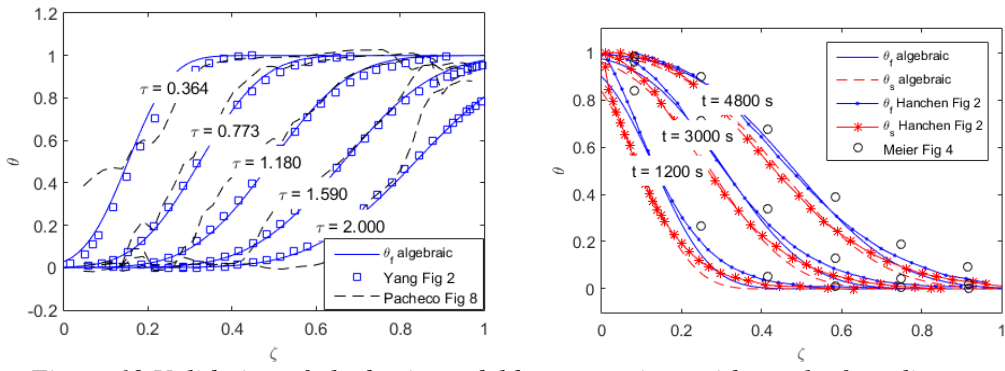


Figure 12 Validation of algebraic model by comparison with results from literature.

Thermocline tank metrics

The tank efficiency can be expressed as the ratio of energy stored (or delivered) during a complete charging (or discharging) cycle, over the total energy that can be stored in the particular tank over the operating temperature range:

$$\eta = \frac{\int_0^{T_{\text{charge}}} \dot{m} C_p (T_{\text{in/out}} - T_{c/h}) dt}{(\rho C_p)_{\text{eff}} V_{\text{tank}} (T_h - T_c)}.$$

Qualitatively, a thinner thermocline implies a steeper gradient between the cold- and hot-fluid regions, and, therefore, higher tank efficiency. Approximating the temperature profile with its maximum slope, the thermocline thickness is solved as $\lambda=1/(\partial\theta_f/\partial\zeta)$, where the maximum slope is found by solving $\partial^2\theta_f/\partial\zeta^2=0$, which occurs for $\zeta=u^*\tau$, where $u^*=\gamma_f Pe$. The tank charging time, τ^* , may be thought of as the time it takes the thermocline, being convected at speed u^* , to cover the length of the tank, e.g. $\zeta=1$, at which time the thickness is given as:

$$\lambda^* = \left[\frac{d_p}{L} \right]^{1/2} \left\{ \frac{4\pi\varepsilon}{\beta_f RePr} + \frac{4\pi\gamma_s^2 RePr}{6(1-\varepsilon)Nu} \right\}^{1/2}.$$

Considering the above definitions of the thermocline thickness and the tank efficiency, the thermocline efficiency may be given analytically as $\eta=1-\lambda^*/2$. Further details are available in [Votyakov 2015].

Sensitivity analysis

The objective of sensitivity analysis is to identify the contribution of the variability of inputs to the variability in the output, hence to find the most important input factor and also the contribution of the variability input interactions [Cannavo 2012].

One approach to this problem is done by computing partial derivatives, varying the inputs one at a time. Such approaches are called one-at-a-time (OAT) and provide measures of local sensitivity. However, the fatal limitation of a derivative-based approach is that it is unwarranted when the model input is uncertain and/or when the model is of unknown linearity, e.g. derivatives are only informative at the base point where they are computed [Saltelli 2008].

To overcome this, global sensitivity analysis methods have been developed, because they deliver global, quantitative and model independent sensitivity measures. Variance based methods are particularly suited as they capture input interactions in non-linear models and can help rank input variables in order of importance [Sobol 2001].

Both one at a time (OAT) and global sensitivity analysis methods were used for the thermocline system. Initially, an OAT screening method was applied to determine the relative importance of the input parameters. Morris' method is chosen as it allows classification of inputs in three categories: those having negligible effect on the output, those with large linear effects but no interactions, and those with large nonlinear and/or interaction effects [Morris 1991, Iooss 2015]. Details of the method are summarized in [Bonanos 2016]. For global sensitivity analysis, the variance based sensitivity analysis was selected, as it is a quantitative variance based technique [Campolongo 2011].

The SAFE toolbox (R1.1, [Pianosi 2015]), implementing both Morris' screening technique and the variance-based sensitivity analysis, was used for the analysis of the thermocline thickness. The thermocline thickness has been shown to be a measure of tank efficiency, and, being an analytical expression, is not computationally costly to evaluate. The thermocline thickness, λ , is expressed as a function of 9 input parameters:

$$\lambda = f(d_p, L, \varepsilon, k_f, k_s, (\rho C_p)_f, (\rho C_p)_s, t, v_f).$$

In the present work we use the dimensional variables in the sensitivity analysis as opposed to the dimensionless groups derived (e.g. Pe , Bi , $\beta_{f,s}$ and $\gamma_{f,s}$). This is because some parameters, such as the tank height, L , appear in the definition of multiple dimensionless parameters and thus it is easier to identify the impact of the specific parameter on the tank performance when it is considered on its own. Since the aim is to provide design guidelines for engineers, it is more useful to identify specific design parameter that highly influence the thermocline thickness, rather than a grouped dimensionless parameter.

The sensitivity analysis methods discussed, being Monte-Carlo statistical methods, require a very large number of function evaluations, and thus the use of an efficient model is required for robust results at a reasonable computational expense.

Range of parameters

Evaluating sensitivity of an output implies knowledge of the range of the input and the distribution within that range. The selected range of input parameters is given in Table 4. The ranges for material properties were derived from a literature survey; a summary of the thermophysical properties of commonly employed materials in thermocline systems is presented in Table 5. Note that in the present work, considerations such as compatibility of solid and filler materials, matching of temperature ranges, and material costs are not taken into account.

Table 4 Range of input parameters for a packed bed thermocline storage tank.

Param.	Min	Max	Nom.	Units
d_p	0.001	0.100	0.01	[m]
L	1	20	10	[m]
ϵ	0.05	0.50	0.22	[–]
k_f	0.01	60	1.0	[W/m-K]
k_s	0.1	200	1.0	[W/m-K]
$(\rho C_p)_f$	1	4.5	2.5	[MJ/m ³ -K]
$(\rho C_p)_s$	1	5.0	2.5	[MJ/m ³ -K]
t	6	12	9	[hours]
v_f	0.05	5	0.5	[μm ² /s]

Table 5 Review of average thermophysical properties of commonly used solid filler and heat transfer fluid materials in packed bed thermocline thermal storage tanks.

Material	ρ [kg/m ³]	C_p [J/kg-K]	ρC_p [MJ/m ³ -K]	k [W/m-K]	T_{min} °C	T_{max} °CC	v_f [m ² /s]
<i>Solid filler materials</i>							
Reinforced Concrete	2200	850	1.87	1.5	200	400	
N4 Concrete	2250	1100	2.475	1.3	200	400	
High Temp. Concrete	2750	916	2.519	1.0			
Cast iron	7200	560	4.032	37	200	400	
Cast steel	7800	600	4.68	40	200	700	
Silica fire bricks	1820	1000	1.82	1.5	200	700	
Magnesia fire bricks	3000	1150	3.45	5	200	1200	
Castable ceramic	3500	866	3.031	1.35			
NaCl (solid)	2160	850	1.836	7	200	500	
Alumina porcelain	2700	880	2.376	2.1		>650	
Graphite	1700	1900	3.23	200		>1500	
Quartzite	2620	620	1.624	3.4		>650	
Limestone	2700	670	1.809	2.5		>650	
Steatite	2680	1068	2.862	2.5		>550	
Cofalit	3120	860	2.683	2.7			
Granite	2893	845	2.445	3			
<i>Heat transfer fluids</i>							
Synthetic oils	850	2200	1.87	1		400	2.5e ⁻⁷
Solar Salt	1790	1500	2.685	0.5	290	590	1.1e ⁻⁶
Saltstream 700e	2000	760	1.52		200	700	5.0e ⁻⁶
LiF-NaF-KF	2000	1890	3.78	0.8	500	1000	4.0 ⁻⁶
Sodium (liquid)	820	1290	1.0578	60	285	873	3.6 ⁻⁷
Lead-Bismuth eutectic	9500	120	1.14	15	285	1650	1.6e ⁻⁷
Supercritical CO ₂ (80 bar, 600 K)	72	1140	0.082	0.04		>850	3.9e ⁻⁷
Pressurized air (20 bar, 600 K)	11.6	1056	0.0122	0.046		>1000	2.6e ⁻⁶

Morris' screening method was applied to the packed bed thermocline thermal energy storage tank model, with the input parameters assumed to vary uniformly in the range identified from the

literature review. Bootstrapping of 100 samples was applied in order to determine the upper and lower bounds of the mean and standard deviation with a significance level of 5%. From the analysis, shown in Figure 13 (left), the following conclusions may be drawn:

- Inputs L, k_s and $(\rho C_p)_s$ have a strong influence with non-linear and/or interaction effects, since m and s are of the same order of magnitude.
- Inputs d_p , k_f , ϵ , $(\rho C_p)_f$ and t have a moderate influence on the output. Further, the order of importance of the variables may not be clearly determined, as the mean has a similar magnitude for these inputs.
- Input v_f has no influence on the model output and may be considered constant.

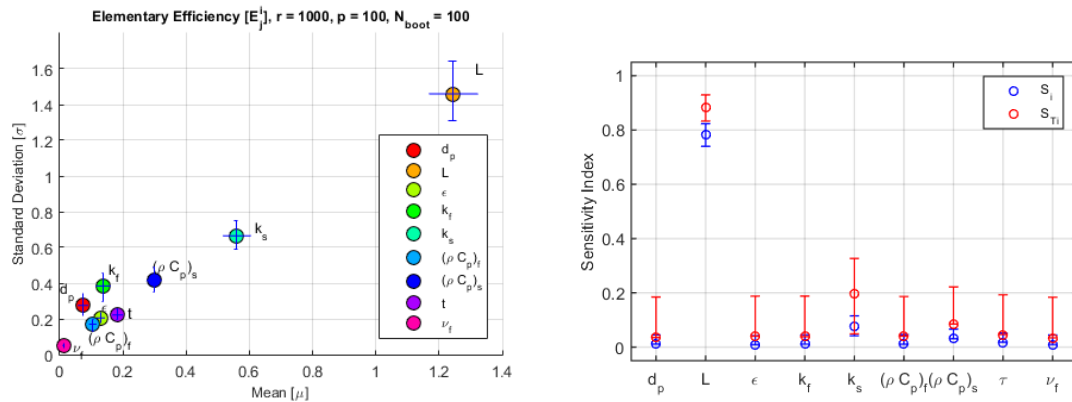


Figure 13 (left) Standard deviation vs. mean of the elementary effects, as evaluated using Morris' screening method. (right) First order and total sensitivity indexes from the Variance Based Sensitivity Analysis

The first-order and total effect sensitivity indexes of the variance based sensitivity analysis were evaluated with a sample size of 10000 and a random uniform sampling strategy. Bootstrapping of 500 samples was applied in order to determine the upper and lower bounds of the sensitivity indexes with a significance level of 5%.

From the analysis, we evaluate $\sum S_i = 0.96$ and $\sum S_{Ti} = 1.40$. A sum of 1 for each index would mean that the model is additive and linear, so this slight deviation implies that some terms have higher order interaction effects. Indeed, this is confirmed in Figure 13 (right), where, for most inputs $S_i \sim S_{Ti}$. Notable exceptions to this are inputs L, k_s and $(\rho C_p)_s$, the same variables identified from the screening method as having the largest influence on the model, thus confirming this result.

The result that the tank height, L, highly influences the thermocline thickness is rather intuitive: the tank height, along with the charging time, dictates the velocity, and therefore whether the process will be dominated by the advective or diffusion term of the energy equation. Given a fixed charging time, a short tank (small L) would result in large thermocline thickness since diffusion will dominate, whereas a tall tank (large L) will maintain a thermocline profile similar to the input step function as it is advected downstream.

The second, and more interesting, result is that the thermocline thickness is far more sensitive to the thermo-physical properties of the solid filler material rather than those of the heat transfer fluid, highlighting the significance of correctly selecting the solid filler material. The analysis shows that in order to minimize the thermocline thickness, the thermal conductivity of the solid, k_s must be as small as possible, whereas the volumetric heat capacity, $(\rho C_p)_s$, must be as large as possible, and that the effect of thermal conductivity is more important than that of the volumetric heat capacity.

Both one-at-a-time and global sensitivity analysis methods agree that the tank height, L, has the largest influence on the thermocline thickness, followed by the thermophysical properties of the

solid filler material, k_s and $(\rho C_p)_s$. The properties of the fluid, the particle size, void fraction and charging times have a secondary influence, whereas the viscosity of the heat transfer fluid does has a negligible effect on the thickness.

References

1. E.V. Votyakov and A.M. Bonanos, “A perturbation model for stratified thermal energy storage tanks”, International Journal of Heat and Mass Transfer, Vol. 75, pp. 218-223, 2014.
2. E.V. Votyakov and A.M. Bonanos, “Algebraic model for thermocline thermal storage tank with filler material”, Solar Energy, Vol. 122, pp. 1154-1157, 2015.
3. Z. Yang and S. Garimella, “Thermal analysis of solar thermal energy storage in a molten-salt thermocline”, Solar Energy, Vol. 84, pp. 974-985, 2010.
4. M. Hanchen, S. Bruckner, A. Steinfeld, “High-temperature thermal storage using a packed bed of rocks – Heat transfer analysis and experimental validation”, Applied Thermal Engineering, Vol. 31, pp. 1798-1806, 2011.
5. F. Cannavo, “Sensitivity analysis for volcanic source modeling quality assessment and model selection”, Computational Geosciences, Vol. 44, pp. 52-59, 2012.
6. A. Saltelli, M. Ratto, T. Andres, F. Campolongo, J. Cariboni, D. Gatelli, M. Saisana, S. Tarantola, “Global Sensitivity Analysis. The Primer”, John Wiley & Sons, 2008.
7. I. Sobol, “Global sensitivity indices for nonlinear mathematical models and their monte carlo estimates”, Math. Comput. Simul. Vol. 55, pp. 271-280, 2001.
8. M. Morris, “Factorial sampling plans for preliminary computational experiments”, Technometrics, Vol. 33, pp. 161-174, 1991.
9. B. Iooss, P. Lemaitre, “A review on global sensitivity analysis methods”, in: C. Meloni, G. Dellino (Eds.), Uncertainty Management in Simulation optimization of Complex Systems: Algorithms and Applications, Springer, 2015.
10. A.M. Bonanos, E.V. Votyakov, “Sensitivity analysis for thermocline thermal storage tank designs”, Renewable Energy Vol. 99, pp. 764-771, 2016.
11. F. Campolongo, A. Saltelli, J. Cariboni, “From screening to quantitative sensitivity analysis: a unified approach”, Comput. Phys. Commun., Vol. 182, pp. 978-988, 2011.
12. F. Pianosi, F. Sarrazin, T. Wagener, “A matlab toolbox for global sensitivity analysis”, Environ. Model. Softw. Vol. 70, pp. 80-85, 2015.

4. PILOT-SCALE DEMONSTRATION AND IMPACT ASSESSMENT

ETH Zurich has contributed with a pilot scale demonstration and with the industrial scale design of a packed-bed thermal storage for CSP, which is described in section 4.1, while SENER has contributed with the impact assessment of using thermoclines with filler in plant operation, which is reported in section 4.2.

4.1 ETHZ contribution: Pilot Scale Demonstration and Industrial Scale Design of a Packed-Bed Thermal Storage for CSP

ETHZ will contribute with a pilot-scale demonstration and industrial-scale design of a packed-bed thermal storage for CSP.

An experimental-numerical approach was used to study combined sensible/latent heat storage based on placing a limited amount of steel-encapsulated AlSi₁₂ on top of a packed bed of rocks. The primary motivation for combining sensible and latent heat storage is to reduce the drop in outflow temperature during discharging that can be observed for sensible heat storage. An unsteady one-dimensional heat-transfer model was verified using exact solutions and validated with experimental data from a 42 kWh_{th} laboratory-scale combined storage. Simulations were then used to compare the performance of 23 MWh_{th} and 1000 MWh_{th} industrial-scale combined and sensible storages.

The simulations showed that the combined storage can reduce the material costs for a given maximum outflow temperature drop during discharging. The simulations also demonstrated that the industrial-scale combined storages meet the goals of exergy efficiencies greater than 95% and material costs below \$15/kWh_{th}.

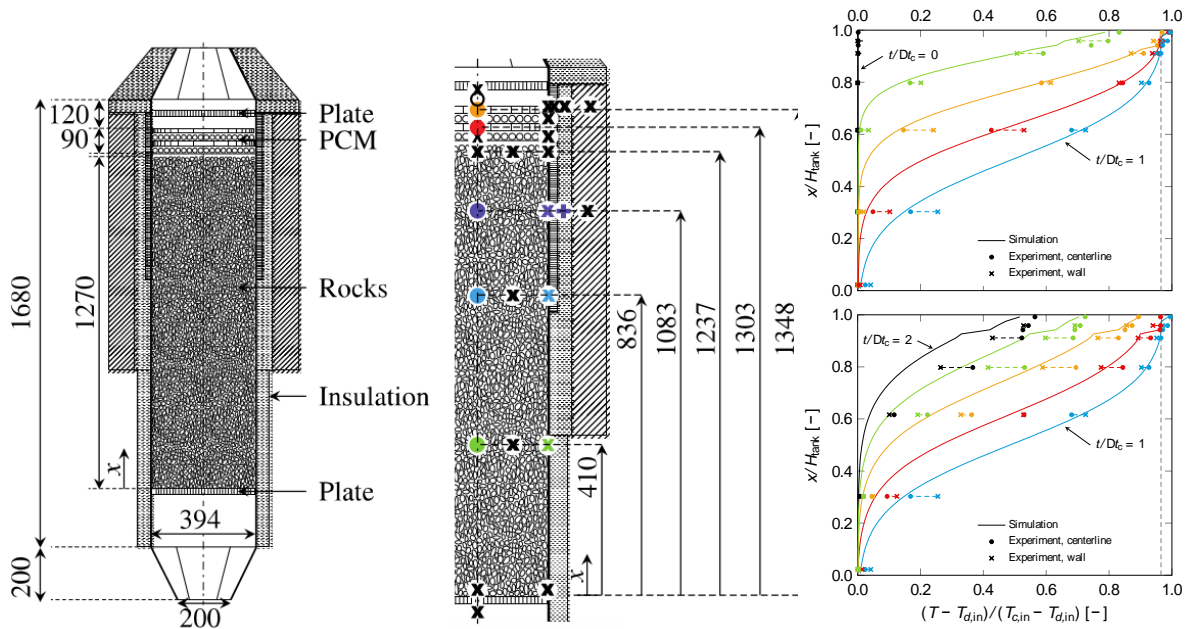


Figure 2: *Left:* Schematic of the laboratory-scale combined sensible/latent heat storage (left) with thermocouple positions indicated by circles and crosses (right). All dimensions in mm. *Right:* Comparison of simulated thermocline with measured centerline and wall temperatures as a function of axial position at selected times during charging (top) and discharging (bottom) for the laboratory-scale combined storage. The shaded region indicates the latent section and the dashed vertical line corresponds to the PCM melting temperature.

Further technical details have been published in [Geissbühler 2016]

References

1. Geissbühler L., Kolman M., Zanganeh G., Haselbacher A., Steinfeld A., "Analysis of industrial-scale high-temperature combined sensible/latent thermal energy storage" Applied Thermal Engineering, Vol.101, pp.657-668, 2016

4.2 SENER contribution: Impact Assessment of using Thermoclines with Filler in Plant Operation

The technology of thermoclines tanks, employing a single thermocline tank, from the investment point of view and in advance from the maintenance point of view, has the potential to replace the traditional and more expensive two tank storage systems.

The thermocline tank approach uses a filler of different materials to displace a significant portion of the volume in the tank. Performances and optimization of these filler materials based on quartzite and basalt are being studied in this task. Then the tank is filled with the heat transfer fluid, a molten nitrate salt. A thermal gradient separates the hot and cold salt. Loading the tank with the combination of filler material and molten salt instead of just molten salt reduces the system cost. This is the approach to the technology from the construction point of view, considering the rest of the systems and subsystems of a typically industrialized thermosolar plant:

- Solar Field.
- Heat Exchangers.
- Steam Generator System (SGS).
- Steam Turbine (ST).
- Condenser.
- Electrical Transformer.
- Cooling System.
- Balance of process (BOP).

Considering only operation issues applying this technology in a classical concept of termosolar plant the critical points of the thermocline tank with filler are as describe below:

- Type and qualities of filler materials must be consider and studied from the durability and reliability point of view.
- In the case of a malfunctioning or being out of service the tank it will be necessary to dispose of a backup tank. A circumstantial problem in the tank will stand for a shutdown of the plant.
- It will be necessary that the filler material and the system have the capability of achieving constant temperatures in order to ensure a constant steam quality.
- It will be necessary to ensure the stability and purity of the filler material. Molten salts going through the filler could sweep along filler particles that could be potentially harmful to the system such as erosion, molten salt degradation,...
- It will be necessary to analyse the impact of energy transfer velocity in plant operation and production during thermocline tank charge and discharge processes.
- It will be necessary to analyse the impact of variation in time of temperature distribution along the thermocline storage component.
- It will be necessary to minimize energy losses and electricity consumption in the thermocline storage tank.
- It will be necessary to define predictive maintenance operations for thermocline storage tank.
- Filler material bed must be either easily for replacing or stable along the whole of operation period.

This list shows some of the most relevant critical points during operation of this kind of technology in a first state of analysis. The analysis and study will be extended when the technology will be more detailed.